

The properties of the high-mass star formation region IRAS 22475+5939

X.-L. Liu^{1,2} and J.-J. Wang¹

¹ National Astronomical Observatories, Chinese Academy of Sciences, Beijing 100012, China; liuxiaolan10@mails.gucas.ac.cn

² Graduate University of the Chinese Academy of Sciences, Beijing, 100080, China

26 March 2012

Abstract IRAS22475+5939 has been well researched by previous astronomers. But we still get some new characteristics about it, using the first observations in lines of CO J = 2 – 1, ¹³CO J = 2 – 1, ¹³CO J = 3 – 2 by the KOSMA 3 m telescope. The mapping of the intensity ratio of, Eiroa 1981, Felli81, Eiroa 1981 ¹³CO J = 3 – 2 and ¹³CO J = 2 – 1 shows the distribution of the temperature with two peaks, which don't coincide with IRAS22475+5939 source and the center of the HII region, but at the edge of the HII region. The overlays of the Spitzer IRAC 8 μ m and CO contours indicate that they are associated with each other and the strongest polycyclic aromatic hydrocarbons (PAHs) emission is at the position of IRAS22475+5939 source. While the IRAS LRS spectrum at 7 μ m ~ 23 μ m and the PHT-s spectrum at 2 μ m ~ 12 μ m of IRAS22475+5939 source also exhibit strong PAHs emission characters at the main PAH bands. The diversity of PAH family should be responsible for the plateaus of PAHs emission in the PHT-s spectrum and the IRAS-LRS spectrum. An analysis and modeling in infrared bands suggest that IRAS22475+5939 is more likely to be a Class I YSO. Where this is the case, the star is likely to have a temperature $T_{\text{EFF}} \sim 9995.8$ K, mass $\sim 15.34 M_{\odot}$, luminosity $\sim 1.54 \times 10^4 L_{\odot}$, and age $\sim 1.54 \times 10^4$ yr. The model shows that the circumstellar disc emission is important for the wavelength between 1 and 10 μ m, otherwise, envelope fluxes for $\lambda > 10 \mu$ m. The bipolar outflow is confirmed in the molecular cloud. The excited star of the HII region has the chance to be the driving source of the outflow. The high resolution is required.

Key words: ISM: jets and outflow — ISM: molecular — ISM: kinematical and dynamics — star formation

1 INTRODUCTION

Researches of massive star formation have been getting significant attention in the recent years. But the mechanism of how massive stars form is still debatable, whether it is through the process similar to that for the low mass stars, i.e., through disk accretion and driving molecular outflows (Shu et al. 1987), or through alternative scenarios-coalescence of low mass stars (Bonnell et al. 1998). But the recent observations show that outflows are common in the massive star formation regions (Zhang et al. 2001) and it is almost clear that stars at least up to late-O spectral types form primarily through disk accretion (Varricatt 2012). HII regions will form when the massive stars ionize their surroundings and provide information about massive star formation within molecular clouds (Heyer et al. 1989; Churchwell 2002). Therefore, the forming stars will have a big influence on their surrounding environment during the

evolutional processes. It is an indirect way to study the properties in the star formation regions in order to know more about how massive stars form.

IRAS22475+5939 has been detected in the sharpness HII region S146 (Zuckerman & Evans 1974). The distance of IRAS22475+5939 from us is about 4.7 kpc (Henkel 1986). Eiroa (1981) believed S146 was excited by an IRS 1, locating at position $\alpha(B1950) = 22^{\text{h}}47^{\text{m}}29^{\text{s}}.7$, $\delta(B1950) = +59^{\circ}38'55'' \pm 7$ at $2.2 \mu\text{m}$, $\alpha(B1950) = 22^{\text{h}}47^{\text{m}}29^{\text{s}}.5$, $\delta(B1950) = +59^{\circ}39'01'' \pm 3$ at $0.9 \mu\text{m}$. Blair (1978) found a H_2O maser associated with IRAS22475+5939. A 2MASS source 22492900+59545600 ($\alpha = 22^{\text{h}}49^{\text{m}}29^{\text{s}}.06$, $\delta = +59^{\circ}54'55''.7$, J2000) was detected by Wang(1997). Felli (1981) showed a bipolar outflow with the optical and 6 cm emissions. The bipolar molecular outflow was also confirmed from surveys of the CO J = 1 – 0 (Yang & Wu 1998), CO J = 2 – 1 (Jiang et al. 2001) and CO J = 3 – 2 (Wu et al. 2005) and Jiang (2001) thought a massive star was forming in the molecular cloud. Guan (2008) made a mapping survey of the massive CO cores with the CO, ^{13}CO , ^{18}CO J = 1 – 0 lines. The contour of ^{13}CO J = 1 – 0 was studied to be associated with MSX $8 \mu\text{m}$ emission (Guan & Wu 2008). The IRAS-LRS (Low Resolution Spectra) spectrum was analyzed by Muizon (1990), Volk (1991) and Chen (1995), respectively. The LRS spectrum shows strong [NeII]($12.8 \mu\text{m}$), [NeIII]($15.5 \mu\text{m}$), [SIII]($18.7 \mu\text{m}$), PAHs emission ($7.7 \mu\text{m}$, $8.6 \mu\text{m}$, $11.3 \mu\text{m}$) as well as the silicate absorption feature at $9.7 \mu\text{m}$ (Muizon et al. 1990; Volk & Kwok 1991; Chen et al. 1995).

In this paper, we show the existence of the outflow and discuss the properties in the observed region. ^{13}CO is optically thin and can trace the internal region of the molecular core. And the intensity ratio $R_{\text{I}_{32/21}}$ (ratio of ^{13}CO J = 3 – 2 and ^{13}CO J = 2 – 1) contains the information about the temperature distribution in the molecular cloud, and mid-infrared emission at $8 \mu\text{m}$ is thought to be from small dust grains and polycyclic aromatic hydrocarbons (PAHs), and excited by the UV radiation leaking from the HII regions (Leger & Puget 1984; Deharveng et al. 2003,2005). We also use the Stokes I image from the observations for the 1.4 GHz NRAO VLA Sky Survey(NVSS) to trace the HII region in order to know the relationship between the molecular cloud, the intensity ratio and the HII region. We describe the observation in section 2. The results and discussion of the properties are in section 3. section 4 makes a conclusion.

2 OBSERVATIONS AND DATA REDUCTION

2.1 The observational data

We carried out observations toward IRAS22475+5939 ($\alpha = 22^{\text{h}}49^{\text{m}}29^{\text{s}}.4$, $\delta = +59^{\circ}54'54''.00$, J2000) source in CO J = 2 – 1, ^{13}CO J = 2 – 1, ^{13}CO J = 3 – 2 lines using the KOSMA 3 m telescope at Gornergrat, Switzerland in April 2004. The half-power beam widths of the telescope at observing frequencies 230.538 GHz, 220.399 GHz, 330.588 GHz are $130''$, $130''$ and $80''$, respectively. The pointing and tracking accuracy is better than $10''$. The DSB receiver noise temperature is about 120 K. The medium and variable resolution acousto-optical spectrometers have 1501 and 1601 channels. The channel widths of 248 MHz and 544 MHz correspond to velocity resolutions of $0.21 \text{ km} \cdot \text{s}^{-1}$ and $0.29 \text{ km} \cdot \text{s}^{-1}$, respectively. The beam efficiency is 0.68 at 230 GHz and 220 GHz, but 0.72 at 330 GHz and 345 GHz. The forward efficiency is 0.93. The $80''$ resolution of the J = 3 – 2 data was convolved to $130''$ with an effective beam size $\sqrt{(130^2 - 80^2)} = 102''$. The correction for the line intensities to the main beam temperature scale was made using the formula $T_{\text{mb}} = (F_{\text{eff}}/B_{\text{eff}} * T_{\text{A}}^*)$. The data were reduced by the software CLASS (Continuum and Line Analysis Single-Disk Software) and GREG (Grenoble Graphic).

2.2 Archival data

The Spitzer IRAC $8 \mu\text{m}$ imaging is available toward the direction of IRAS22475+5939 at an angular resolution of $\sim 2''$. S146 was detected well by the 1.4 GHz NRAO VLA Sky Survey(NVSS). Its resolution is $45''$ and a limiting peak source brightness is about 2.5 mJy/beam. We have compiled the SED for IRAS22475+5939 source using near-IR (JHK) flux from the 2MASS All-Sky Point Source

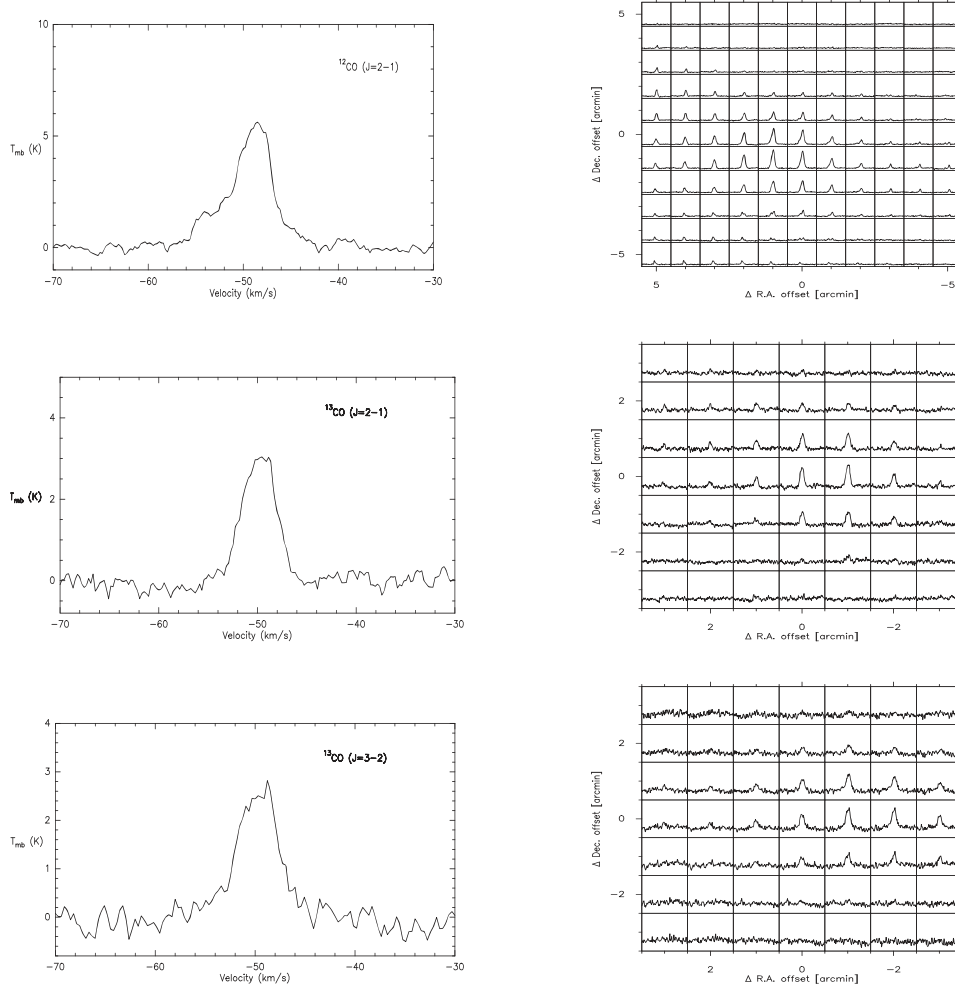


Fig. 1 Left: spectra of CO ($J = 2 - 1$), ^{13}CO ($J = 2 - 1$) and ^{13}CO ($J = 3 - 2$) at the position of (-1, 0). Right: channel maps of the corresponding isotopes

Catalog (PSC), mid-IR MSX four bands from the Midcourse Space Experiment (MSXC6), and the IRAS data from IRAS Point Source Catalog v2.1 (PSC). The IRAS LRS spectrum is obtained from the LRS database at the University of Calgary¹ (Hodge et al. 2004;Kwok et al.1997). The LRS was a slitless spectrometer and well-suited to point sources whereas confusion arises in the case of extended source. Two wavelength channels are recorded simultaneously: Band 1 ($7.7 - 13.4 \mu\text{m}$) and Band 2 ($11.0 - 22.6 \mu\text{m}$). The wavelength resolution $\lambda/\Delta\lambda$ varies between 10 and 60; it increases with wavelength inside each wavelength band, the resolution being systematically somewhat lower in band 2 than in band 1. PHT-s consist of a dual grating spectrometer with two 64-element arrays that span the $2.5 - 4.9 \mu\text{m}$

¹ See <http://www.astro.wisc.edu/protostars>

and 5.8–11.6 μm spectra regions. The Auto Analysis Result produced by the Off-Line Processing (OLP) from the ISO Data Archive (IDA) is available (Hodge et al. 2004; Lemke et al. 1996)

3 RESULTS AND DISCUSSION

3.1 The outflow

3.1.1 The molecular spectral lines

Figure 1 shows the spectra and channel maps of CO $J = 2 - 1$, $^{13}\text{CO } J = 2 - 1$, $^{13}\text{CO } J = 3 - 2$. The spectra are at the positions (-1,0). Each spectrum shows a broad width as well as the almost same V_{LSR} and shape. The showing spectra are the strongest for $^{13}\text{CO } J = 2 - 1$, $^{13}\text{CO } J = 3 - 2$. The optically thick line CO $J = 2 - 1$ is not gaussian shape and has wings. The blue wing and the red wing are not asymmetrical. Table 1 presents the observational parameters of IRAS22475+5939 source. The ranges of the FW come from P-V diagram, which shows the high-velocity gas exists.

Table 1 Observation physical parameters of IRAS22475+5939 Source

Name	T_{mb} (K)	FWHM ($\text{km} \cdot \text{s}^{-1}$)	FW ($\text{km} \cdot \text{s}^{-1}$)	V_{LSR} ($\text{km} \cdot \text{s}^{-1}$)
CO ($J = 2 - 1$)	11.20	4.99 ± 0.03	12.37	-49.60 ± 0.01
^{13}CO ($J = 2 - 1$)	3.02	3.90 ± 0.08	6.33	-49.80 ± 0.04
^{13}CO ($J = 3 - 2$)	2.55	4.79 ± 0.17	7.87	-49.69 ± 0.07

3.1.2 The outflow and its physical parameters

Table 2 Physical parameters of the outflow

Name IRAS	Wing	$N(\text{H}_2)$ ($\times 10^{20} \text{cm}^{-2}$)	M (M_{\odot})	t_d ($\times 10^5 \text{yr}$)	\dot{M} ($\times 10^{-6} M_{\odot} \text{yr}^{-1}$)
22475 + 5939	blue	1.00	278.79	5.37	3.86
	red	0.15	26.63	3.25	0.80
Name IRAS	Wing	F ($M_{\odot} \text{kms}^{-1} \cdot \text{yr}^{-1}$)	P ($M_{\odot} \text{kms}^{-1}$)	E ($\times 10^{46} \text{erg}$)	L_{Mech} (L_{\odot})
22475 + 5939	blue	1.93×10^{-3}	1028.74	7.59	1.17
	red	3.99×10^{-4}	129.699	1.26	1.23

We show the outflow and its corresponding P-V diagram in Figure 2. The integrated ranges of the blue wing and the red wing are determined by the P-V diagram and gaussian fit. We find they overlap with each other, which is likely they are in the direction of the sight or the resolution of the telescope is too low to identify the direction of the outflows. And IRAS22475+5939 as well as its associated H_2O maser are almost in the center of the wings. Maybe IRAS22475+5939 is the driving source of the outflow. The physical parameters are presented in Table 2. Assuming it is local thermodynamic equilibrium (short for LTE latter) and CO in the outflow is optically thin, we can calculate the column density of the outflow using the below formula (Scoville et al. 1986) under the assumption of $N(\text{CO})/N(\text{H}_2) \approx 10^{-4}$ (Dickman et al. 1978):

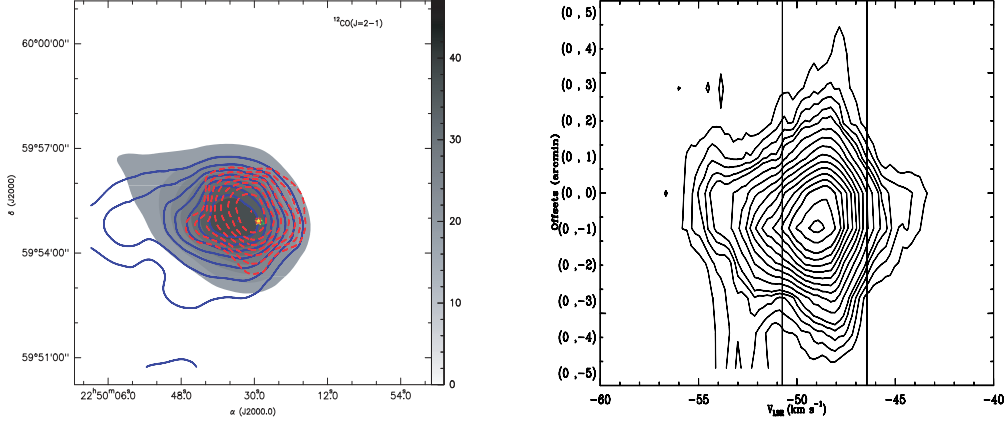


Fig. 2 Left panel: outflow contours of CO ($J = 2 - 1$), the integrated ranges in blue wing and red wing are $-55.78 \text{ km} \cdot \text{s}^{-1} \sim -50.80 \text{ km} \cdot \text{s}^{-1}$, $-46.05 \text{ km} \cdot \text{s}^{-1} \sim -43.41 \text{ km} \cdot \text{s}^{-1}$, respectively. The contour levels are 30% \sim 90% of each wing's peak value. The star is IRAS22475+5939, the triangle is the H₂O maser, and the square is the 2MASS source 22492900+59545600. Right panel: P-V diagram. The contour levels are 0.7 \sim 3 by 0.6 K, 3 \sim 12 by 1.0 K, 12 \sim 20 by 1.5 K. The vertical lines indicate the beginning of the blue and red wings, respectively.

$$N = 10^5 \times \frac{3k^2}{4h\pi^3\mu^2\nu^2} \exp\left(\frac{h\nu J}{2kT_{\text{ex}}}\right) \frac{T_{\text{ex}} + h\nu/6k(J+1)}{\exp(-h\nu/kT_{\text{ex}})} \times \int \frac{\tau}{1 - e^{-\tau}} T_{\text{mb}} dv \quad (1)$$

where T_{ex} is the excited temperature, which is got from the equ(9). J is the lower level of the transition. $\mu = 0.112 \text{ D}$.

The other physical parameters coming from the below formulas (Xu & Wang 2010) :

$$M = \mu m_{\text{H}_2} SN(\text{H}_2)/2 \times 10^{33} \quad (2)$$

$$P = MV \quad (3)$$

$$E = MV^2 \quad (4)$$

$$t_d = R/V \quad (5)$$

$$F = P/t_d \quad (6)$$

$$\dot{M} = P/t_d v_w \quad (7)$$

$$L_{\text{Mech}} = E/t_d \quad (8)$$

where M is the outflow's mass, t_d , P , E , V , R , F , L_{Mech} are the dynamic time, the momentum, the energy, the mean velocity of the gas relative to the V_{LSR} , the size of the wings, the driving force, the mechanical luminosity. The mean atomic weight of the gas $\mu = 1.36$, S is the area of the outflow. From these parameters, we can see the outflow is massive and energetic than the low-mass stars, so we further validate that it is possible to have massive stars forming in this region. At the same time, through the outflow and its parameters, we find the blue outflow is far larger than the red one, and both are elongated from east to west, very similar to the ¹³CO $J = 3 - 2$ molecular core that is presented latter. The explanation is that the surrounding gas might mix with the blue wing. But we can not make sure because of the low resolution of the telescope.

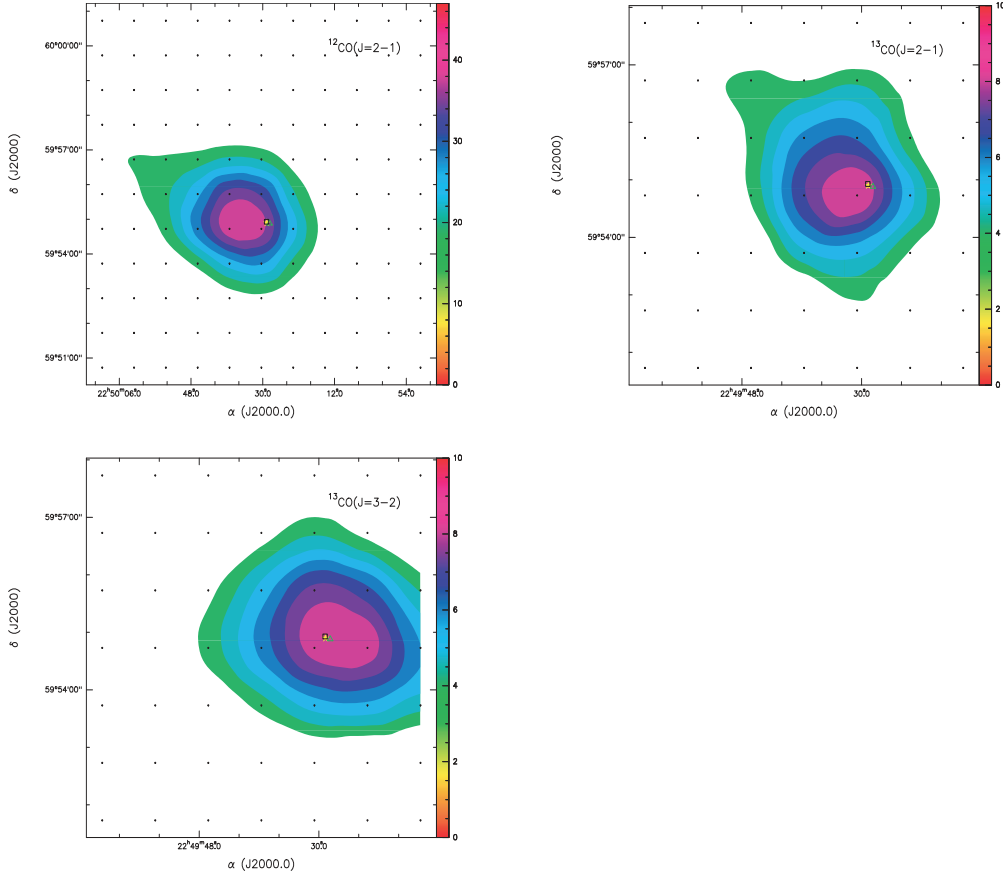


Fig. 3 Integrated intensity diagrams of the core emission. In each map, the integrated range is from $-50.80 \text{ km} \cdot \text{s}^{-1}$ to $-46.05 \text{ km} \cdot \text{s}^{-1}$. The contour levels are 30% to 90% of the peak value.

3.2 The molecular core

Figure 3 shows the structure of the molecular core. The integrated range is determined by the P-V diagram and the gaussian fit due to the relatively large noise. It is more accurate than one determined by each of them. In the diagrams, we find the core structure from $^{13}\text{CO } J = 3 - 2$ is elongated from east to west, but almost round from the transition $\text{CO } J = 2 - 1$, $^{13}\text{CO } J = 2 - 1$. IRAS 22475+5939 and H_2O maser coincide with the peak of cores. We also calculate the core's physical parameters by the expressions (Garden et al. 1991) under the assumption of LTE:

$$T_{\text{ex}}(\text{CO}) = \frac{h\nu}{k} \left(\ln \left(1 + \frac{h\nu}{k} \left[\frac{T_{\text{mb}}}{f} + \frac{h\nu/k}{\exp(h\nu/kT_{\text{bg}}) - 1} \right]^{-1} \right) \right)^{-1} \quad (9)$$

$$\tau(^{13}\text{CO}) = -\ln \left\{ 1 - \frac{kT_{\text{mb}}}{h\nu} \left[\frac{1}{\exp(h\nu/kT_{\text{ex}}) - 1} - \frac{1}{\exp(h\nu/kT_{\text{bg}}) - 1} \right]^{-1} \right\} \quad (10)$$

where $T_{\text{bg}} = 2.732 \text{ K}$ is the temperature of the cosmic background radiation, f is the beam filling factor, here we assuming $f = 1$. Assuming $\tau(\text{CO})/\tau(^{13}\text{CO}) = [\text{CO}]/[^{13}\text{CO}] = 89$ (Lang et al.1980). We can

use another method to calculate the optical depths:

$$\frac{T_{\text{mb}}(\text{CO})}{T_{\text{mb}}(^{13}\text{CO})} = \frac{1 - \exp[-\tau(\text{CO})]}{1 - \exp[-\tau(^{13}\text{CO})]} \quad (11)$$

The two calculated values are summarized in Table 3. Comparing with them, we find they are the same in the error scale. Therefore we can draw a conclusion that our assumptions are right and the abundance ratio $[\text{CO}]/[^{13}\text{CO}]$ in this region is almost the same as in our solar system. The core's physical parameters are in Table 4. From the figures and tables, we can know that the core is isolated and massive, which can provide the environment for the high-mass star formation.

Table 3 Calculated results of the optical depth by two methods

Name	τ_1	τ_2
$^{13}\text{CO}(J = 2 - 1)$	0.28	0.28

Notes: τ_1 is derived from the fist method, τ_2 is from the second method.

Table 4 Physical parameters of the core

Name	T_{ex} (K)	τ	$N(\text{CO}J = 2 - 1)$ ($\times 10^{18}\text{cm}^{-2}$)	$N(\text{H}_2)$ ($\times 10^{22}\text{cm}^{-2}$)	M ($\times 10^3 M_{\odot}$)
IRAS22475 + 5939	17.35	24.92	1.03	1.03	3.56

3.3 The intensity ratio $R_{I_{32/21}}$

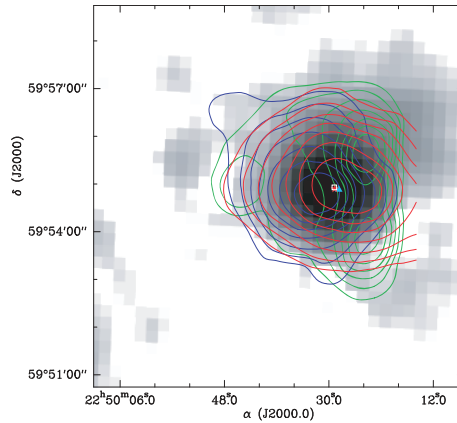


Fig. 4 Grayscale shows the 1.4 GHz NVSS image. The intensity ratio $R_{I_{32/21}}$ is the green contour, the blue and red contours are the integrate intensity maps of $^{13}\text{CO}(J = 2 - 1)$, $^{13}\text{CO}(J = 3 - 2)$, respectively. The star is IRAS22475+5939, the triangle is the H_2O maser, and the square is the 2MASS source 22492900+59545600.

Figure 4 gives the contours of ^{13}CO and the intensity ratio $R_{I_{32/21}}$ overlapping on the 1.4 GHz NVSS grayscale diagram which can trace the structure of the radio source, here we can identify the

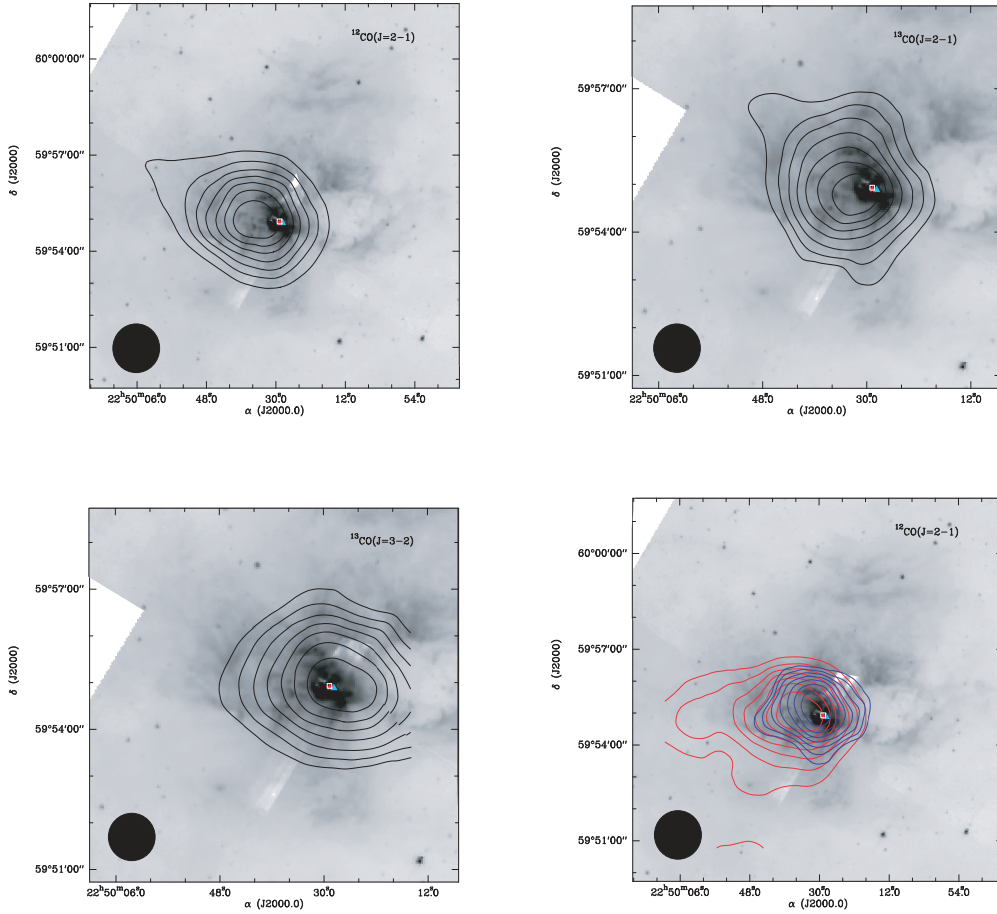


Fig. 5 The molecular cores from the transitions $\text{CO}(J = 2 - 1)$, $^{13}\text{CO}(J = 2 - 1)$, $^{13}\text{CO}(J = 3 - 2)$ (top left, top right, bottom left) and the outflow of $\text{CO}(J = 2 - 1)$ emission (bottom right) overlaid on the grayscale Spitzer $8\ \mu\text{m}$ emission. The synthesized beam size ($\sim 1'$) is shown in the lower left-hand corner of the each panel of KOSMA 3m telescope.

radio source is a HII region (Lockman et al. 1989). The intensity ratio indicates the gas temperature distribution in the region (Qin et al. 2008). From Fig 4, we can find the morphology of the intensity ratio map is similar to a triangle and has three peaks. The peaks are not in the center of the molecular cloud core, the biggest peak is in the northwest, about $2'$ away from the center. The value of it is $\sim 2.12 > 1$, which is bigger than the value (< 1) detected in Cepheus B (Beuther et al. 2000). Maybe it is related with HII regions (Wilson et al. 1997). The second peak and the third peak are in the direction of southwest and east, respectively. All of three are at the edge of the HII region. This shows the temperature at the edge is higher than the center. Maybe the hot gas of the molecular cloud was pushed away to the edge and heated by the HII region. This explanation can be supported by the distribution of the HII region and the molecular core. Additionally, we find ^{13}CO higher J can trace the warmer region. And the center of the molecular core coincides with that of the HII region.

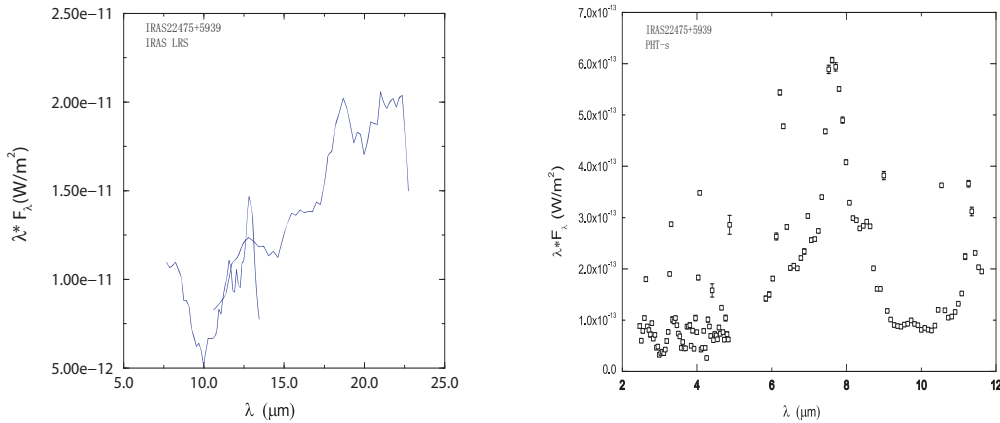


Fig. 6 Left panel: the IRAS-LRS spectrum coming from LRS database at the university of Calgary, consistent of two wavelength band: $7.7 - 13.4 \mu m$, $11.0 - 22.6 \mu m$. Right panel: the PHT-s spectrum lying in the $2 - 12 \mu m$ range.

3.4 polycyclic aromatic hydrocarbons (PAHs)

Fig 5 shows the superposition diagrams of the CO isotopes' contours and CO outflow on the Spitzer $8 \mu m$ emission. The Spitzer IRAC $8 \mu m$ emission is primarily due to the $7.7 \mu m$ and $8.6 \mu m$ PAHs features. The grayscale diagram shows the distribution of PAHs in the HII region. We can see that the strongest PAHs emission coincides with IRAS22475+5939 source, which shows the PAHs emission probably is excited by the UV radiation from IRAS22475+5939.

Fig 6 shows the LRS spectrum and the PHT-s spectrum, spanning the wavelength $7.7 - 23 \mu m$ and $2 - 12 \mu m$, respectively. They are dominated by PAHs emission features at the so-called unidentified infrared bands ($3.3, 6.2, 7.7, 8.6, 11.2 \mu m$) and weaker bands²(Peeters 2011). The PHT-s spectrum shows the narrow and strongest emission at $7.6 \mu m$ at the wavelength range $2 - 12 \mu m$ and an absorption at $9.7 \mu m$, but the strongest emission for the LRS is at $12.0 \mu m$ at band 1. It is more believable for the PHT-s due to its higher resolution than the results of the LRS. And a broad emission plateau at $16.4 - 17.4 \mu m$ maybe resolute from the low resolution or the diverse PAH family. Muizon (1990) pointed out that the prominent emissions at $12.8, 15.55, 18.7 \mu m$ are [NeII], [NeIII], [SIII] lines, respectively.

3.5 The spectral energy distribution

Table 5 Results from SED fitting

Parameter	SM (M_{\odot})	age (yr)	T_{EFF} (K)	DM (M_{\odot})	Disk accretion rate ($M_{\odot} \text{yr}^{-1}$)	Luminosity L_{\odot}	A_{ν}
Best fit values	15.34	1.54×10^4	9995.8	0.13	1.56×10^{-5}	1.54×10^4	4.53

Notes: SM is short for stellar mass, DM is for disk mass, the luminosity is the total luminosity of the star, A_{ν} is the foreground extinction. The best fit values are derived the average values for the best top 10 models.

The 2MASS, MSX, and IRAS data are used to construct the SED of the IRAS22475+5939 source. Color correction is applied to the IRAS data using the correction factors given in the point source

² This includes bands at $3.4, 3.5, 5.25, 5.75, 6.0, 6.6, 6.9, 7.2 - 7.4, 8.2, 10.5, 10.8, 11.0, 12.0, 13.5, 14.2, 15.8, 16.4, 16.6, 17.0, 17.4, 17.8, 19.0 \mu m$

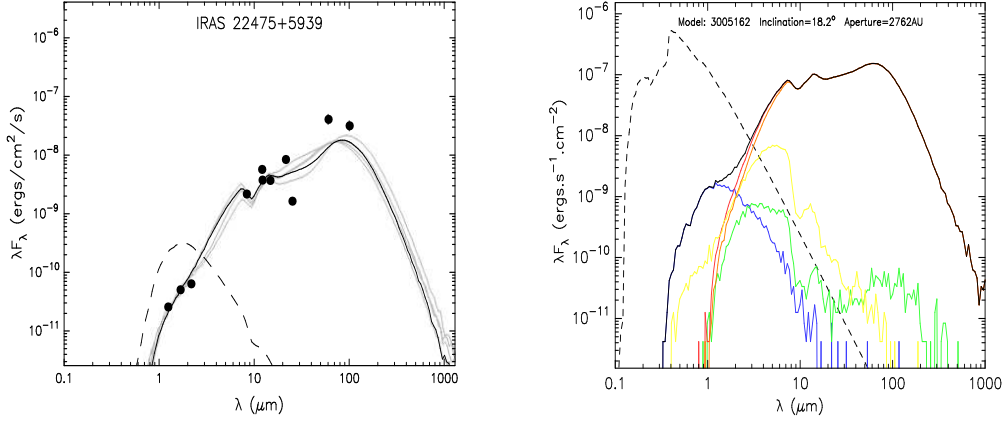


Fig. 7 Left panel: the SED of the IRAS 22475+5939 source. The filled circles show the data from 2MASS (JHK), MSX (ACDE), IRAS (12, 25, 60, 100 μm). The continuous line shows the best fit model and the grey lines show subsequent good fits for $(\chi^2 - \chi_{best\,fit}^2)$ per data point < 3 . The dashed line corresponds to the stellar photosphere for the central source of the best fitting model, as it would look in the absence of the circumstellar (but including interstellar extinction). Right panel: various emission components making up this model, details in the text. Suffice to remark that the circumstellar disc (green curve) is important for wavelengths between 1 and 10 μm .

catalogue (Beichman et al. 1988). The SED fitting tool of Robitaille et al. (2007) is available on-line to model the SED. The SED plot is showed in Fig 7 and its fitting parameters in Table 5. We derived a mass, luminosity and temperature of $15.34 M_{\odot}$, $1.54 \times 10^4 L_{\odot}$, 9995.8 K respectively from the fit. And the average foreground extinction is ~ 4.53 . From the SED and the active accreting mass, IRAS22475+5939 is probably to be a class I protostar.

We have also indicated the differing component of flux which make up the model YSO spectrum (right panel of Fig 7). In this case, the total flux is indicated as black, the stellar flux as blue, the stellar photospheric flux is showed in the dashed line (this is the flux prior to reddening by circumstellar dust), the disc flux as green, the scattered flux as yellow, the envelope flux as red and the thermal flux as orange. Unless otherwise stated, the results include the effects of circumstellar extinction, but not of IS extinction. The also assume a representative distance of 1 kpc.

It is apparent, from the latter modeling, that the central star and disc components of emission are responsible for the MIR/NIR emission, but envelope fluxes are of most importance at $\lambda > 10 \mu\text{m}$.

3.6 Discussion

The morphology of the cores are firstly showed from the lines $\text{CO } J = 2 - 1$, $^{13}\text{CO } J = 2 - 1$, $^{13}\text{CO } J = 3 - 2$, as well as the corresponding parameters. Comparing with the results in CO, ^{13}CO , $^{18}\text{CO } J = 1 - 0$ (Guan et al. 2008), the V_{LSR} and the derived physic parameters are litter difference. And the structure of $^{13}\text{CO } J = 1 - 0$ detected by them is similar to $^{13}\text{CO } J = 2 - 1$. The outflow traced by $\text{CO } J = 2 - 1$ is more extended than that of $\text{CO } J = 3 - 2$ (Jiang et al. 2001). Yang(1998) only analyzed the IRAS data and obtained that IRAS22475+5939 may be a massive YSO with high luminosity. Due to the SED in infrared bands, we suggest that IRAS22475+5939 is likely to be a class I YSO with mass $15.34 M_{\odot}$, luminosity $1.54 \times 10^4 L_{\odot}$, age $1.54 \times 10^4 \text{ yr}$, $T_{\text{EFF}} 9995.8 \text{ K}$. Its foreground extinction is about 4.53 mag. Muizon (1990) suggests the PAH characteristics at 7.7, 8.6, 11.3 μm , silicate absorption features at 9.7 μm and the prominent emissions at 12.8 μm ([NeII]), 15.55 μm ([NeIII]), 18.7 μm ([SIII]) according to

the IRAS-LRS spectrum. But we combine the IRAS-LRS spectrum with the PHT-s spectrum, finding the PAHs emissions are showed at all the PAH bands, especially at the main PAH bands (3.3, 6.2, 7.7, 8.6, 11.2 μm) and 16.4 – 17.4 μm . This indicates the diverse PAH family in the molecular cloud. The HII region is likely to be excited by IR1-an O7V-O7.5V star (Eiroa et al.1981). Its position almost coincides with IRAS22475+5939. Therefore, the star has the chance to drive the outflow. It is necessary to have high resolution observation to identify their relationship.

4 CONCLUSION

We observed the IRAS22475+5939 source using three spectral lines CO J = 2 – 1, ^{13}CO J = 2 – 1, ^{13}CO J = 3 – 2. The V_{SLR} of them are almost the same. The massive and energetic outflow is further verified by us, showing that this region is a high-mass star formation region. The integrated intensity maps of the cores tell us the molecular cloud is isolated. And the core's mass is larger than the low-mass cores. The intensity ratio $R_{\text{I}_{32/21}}$ map indicates the gas temperature varies at different positions and the maximum value is bigger than 1, which is larger than the regions without HII regions (Wilson et al. 1997). And the peaks of the intensity ratio are at the edge of the HII region. Maybe the HII region blows away the hot molecular gas from the center to the edge and heats the gas. This causes the temperature is higher at the edge than the center of the molecular core. And ^{13}CO higher J transition traces the warm regions. PAH features are demonstrated in the Spitzer IRAS 8 μm emission and the spectra of IRAS-LRS and PHT-s, suggesting a rich PAH molecules in the cloud. IRAS22475+5939 may be a massive and luminous class I protostar with a active disc. But considering the position of the excited star of the HII region, the excited star is able to drive the outflow. Maybe it is the driving source of the outflow. The high resolution observations is needed for better results.

Acknowledgements: We would like to thank Drs. Sheng-Li Qin and Martin Miller for the data acquisition. This research has made use of the data products from the 1.4 GHz NRAO VLA Sky Survey (NVSS), and also used the NASA/IPAC Infrared Science Archive, which is operated by the Jet Propulsion Laboratory, California Institute of Technology, under contract with the National Aeronautics and Space Administration. IRAS, MSX, 2MASS photometry are download from the NASA/IPAC Infrared Science. We thank SUN Kwok for providing the LRS database at the University of Calgary. ISOPHOT data was obtained from the ISO Data Archive(IDA), tanks to Lemke, D. for his reducing to the PHT-s data.

References

- Beichman, C.A., Neugebauer, G., Habing, H.J., Clegg, P.E., & Chester, T.J. 1988, Infrared astronomical satellite (IRAS) catalogs and atlases. Volume 1: Explanatory supplement, 1,
 Beuther, H., Kramer, C., Deiss, B., & Stutzki, J. 2000, A&A, 362, 1109
 Blair, G.N., Davis, J.N., Dickinson, D.F. 1978, ApJ, 226, 435
 Bonnell, I.A., Bate, M. R., & Zinnecker, H. 1998, MNRAS, 298, 93
 Chen, P.S., Gao, H., & Xiong, G.Z. 1995, ApJS, 100, 389
 Churchwell, E. 2002, ARA&A, 40, 27
 Deharveng, L., Zavagno, A., Salas, L., et al. 2003, A&A, 399, 1135
 Deharveng, L., Zavagno, A., & Caplan, J. 2005, A&A, 433, 565
 Dickman, R.L. 1978, ApJS, 37, 407
 Eiroa, C., Neckel, T., Sanchez Magro, C., & Selby, M. J. 1981, A&A, 95, 206
 Felli, M., Harten, R.H. 1981, A&A, 100, 42
 Guan, X., Wu, Y., & Ju, B. 2008, MNRAS, 391, 869
 Guan, X., Wu, Y.F. 2008, ChJAA (Chin. J. Astron. Astrophys.), 8, 230
 Garden, R.P., Hayashi, M., Hasegawa, T., Gatley, I., & Kaifu, N. 1991, ApJ, 374, 540
 Henkel, C., Gusten, R., & Haschick, A.D. 1986, A&A, 165, 197
 Heyer, M.H., Snell, R. L., Morgan, J., & Schloerb, F.P. 1989, ApJ, 346, 220
 Hodge, T.M., Kraemer, K.E., Price, S.D., & Walker, H.J. 2004, ApJS, 151, 299

- Jiang, L.J., Wu, Y.F., Miller, M. 2001, *China Academic Journal*, 46, 18
- Kwok, S., Volk, K., & Bidelman, W. P. 1997, *ApJS*, 112, 557
- Lang, K.R. 1980, *Science*, 207, 174
- Leger, A., Puget, J.L. 1984, *A&A*, 137, L5
- Lemke, D., Klaas, U., Abolins, J., et al. 1996, *A&A*, 315, L64
- Lockman, F.J. 1989, *ApJS*, 71, 469
- Jourdain de Muizon, M., Cox, P., & Lequeux, J. 1990, *A&AS*, 83, 337
- Peeters, E. 2011, *EAS Publications Series*, 46, 13
- Qin, S.L., Wang, J.J., Zhao, G., Miller, M., Zhao, J.H., *A&A*, 484, 361-369
- Robitaille, T.P., Whitney, B. A., Indebetouw, R., & Wood, K. 2007, *ApJS*, 169, 328
- Scoville, N.Z., Sargent, A.I., Sanders, D.B. et al. 1986, *ApJ*, 303, 416
- Shu, F.H., Adams, F.C., & Lizano, S. 1987, *ARA&A*, 25, 23
- Varricatt, W.P. 2012, arXiv:1202.4795
- Volk, K., Kwok, S., Stencel, R.E., & Brugel, E. 1991, *ApJS*, 77, 607
- Wang, J. 1997, Ph.D. thesis, Beijing Astro. Obs.
- Wilson, C.D., Walker, C.E., Thornley, M.D. 1997, *ApJ*, 483, 21
- Wu, Y., Zhang, Q., Chen, H., Yang, C., Wei, Y., Ho, P.T.P. 2005, *The Astronomical Journal*, 129:330-347
- Xu, J.L., Wang, J.J. 2010, *RAA*, 10, 2
- Yang, C.Y., Wu, Y.F. 1998, *ACTA ASTROPHYSICA SINICA*, 18, 3
- Zhang, Q., Hunter, T.R., Sridharan, T.K., & Ho, P.T.P. 2001, *Bulletin of the American Astronomical Society*, 33, #134.13
- Zuckerman B, Evans N III 1974, *ApJ*, 192, 149